JETIR.ORG ISSN: 2349-5162 | ESTD Year : 2014 | Monthly Issue
JOURNAL OF EMERGING TECHNOLOGIES AND INNOVATIVE RESEARCH (JETIR)
An International Scholarly Open Access, Peer-reviewed, Refereed Journal

COMPARATIVE BATCH ADSORPTION STUDY OF MICRO AND NANO BALL-MILLED BAMBOO ACTIVATED CARBON FOR REMOVAL OF REMAZOL BRILLIANT ORANGE-3R DYE

[1]Vaishali S. Mohite, [2]Pravinkumar D. Patil,
[1]Assistant Professor [2]Professor
School of Engineering and Technology, Shivaji University, Kolhapur, Maharashtra, India

Abstract: The adsorption of Remazol Brilliant Orange-3R (RBO-3R) dye onto bamboo stick activated carbon prepared at 600 °C (BSAC600) was studied in batch mode, comparing micro-sized BSAC with its nano ball-milled form (N-BSAC). Characterization by SEM, FTIR, and XPS confirmed that ball milling reduced particle size, increased surface roughness, and enhanced the presence of oxygen-containing functional groups. Batch adsorption experiments were conducted to investigate the effects of pH, temperature, contact time, initial dye concentration, and adsorbent dose. Compared with micro-BSAC, N-BSAC exhibited faster kinetics and higher dye removal efficiency. Equilibrium data fitted well to the Langmuir isotherm, yielding a substantially higher maximum adsorption capacity for N-BSAC. Kinetic analysis followed the pseudo-second-order model, indicating chemisorption as the rate-controlling mechanism. Thermodynamic parameters confirmed that the process was spontaneous and endothermic. These findings demonstrate that nano ball milling significantly enhances the performance of bamboo-based activated carbon, establishing N-BSAC as a sustainable and effective adsorbent for textile dye removal..

Keywords: Adsorption, Bamboo stick activated carbon, Nano ball milling, Remazol Brilliant Orange-3R, Kinetics., Isotherms, Thermodynamics, Wastewater treatment.

I. INTRODUCTION

The discharge of synthetic colours from the textile and dye industries, which are often hazardous, non-biodegradable, and resistant to standard treatment techniques, poses a significant environmental risk. When released into natural water bodies without treatment, reactive dyes like Reactive Blue Orange 3R (RBO-3R) can be harmful to human health in addition to adding vibrant colour [1,2]. Adsorption is the most popular treatment approach due to its ease of use, affordability, and broad range of applications [3,4].

One of the most often utilized adsorbents for dye removal is activated carbon. Surface area, porosity, particle size, and surface functional groups all affect how effective activated carbon is. Bamboo's quick growth, high cellulose content, and accessibility make it a suitable precursor for activated carbon [5]. Furthermore, the porosity and surface chemistry are greatly influenced by the carbonization temperature; for instance, BSAC made at 600 °C has a tendency to develop large porosity, which makes it a good application for dye adsorption.

By increasing surface area, decreasing diffusion channel lengths, exposing more active sites, and enhancing external mass transfer, adsorption performance can be improved by reducing adsorbent particle size to the micro- or nano-scale. A mechanical technique for reducing particle size and causing structural changes is ball milling. According to earlier research [5,6] activated carbon derived from bamboo that has been ball-milled to the nanoscale exhibits modified functional group exposure, increased surface area, and a changed pore radius.

This study examines bamboo stick activated carbon (BSAC-600 °C) in micro- and nano-sized additions. It shows that, under different batch conditions, nano ball milling greatly improves the adsorption capacity and kinetics for the removal of Remazol Brilliant Orange 3R dye. The textile industry's enormous release of colored effluents containing permanent dyes like Remazol Brilliant Orange 3R causes serious environmental issues. In contrast to its micro-sized relative, bamboo stick activated carbon (BSAC-600 °C), this study shows that nano ball milling greatly improves its adsorption efficiency, kinetics, and thermodynamic favourability. The findings suggest a cost-effective and sustainable approach to developing innovative adsorbents for the treatment of textile wastewater [7,8,9].

II. MATERIALS AND METHODS

2.1 Materials

Locally produced Managa bamboo was collected from Kolhapur, IndiaAfter properly cleaning the sticks with distilled water to remove any remaining dirt or contaminants, they were oven-dried for 24 hours at 105°C. Before activation, the dried bamboo was cut into 2-3 cm pieces.

Remazol Brilliant Orange 3R (RBO-3R; $C_{20}H_{17}N_3Na_2O_{11}S_3$), an analytical-grade azo dye that was obtained from a local Kolhapur supplier, was used as the adsorbate in the present research. For the production of carbon, ortho-phosphoric acid (H_3PO_4, 85% purity) was used as the activating agent. The pH was adjusted using sodium hydroxide (NaOH) and hydrochloric acid (HCl), and all solutions were prepared using double-distilled water

2.2 Preparation of Bamboo Stick Activated Carbon

Chemical Impregnation

Before chemical impregnation, a portion of the dried bamboo sticks was ground into a powder. The powder was reduced to a nano size by using a planetary ball mill for 30 minutes at 500 rpm. Ortho-phosphoric acid was then used to chemically activate the bamboo particles, both with and without nanoball milling. A 1:1 (w/w) bamboo-to-acid impregnation ratio was maintained. To ensure complete impregnation, the liquid was continually mixed for four hours before being let to soak for twenty-four hours at room temperature.

Thermal Activation

After being moved to a muffle furnace, the impregnated samples were thermally activated for two hours at 600 °C. To provide an inert atmosphere and avoid combustion, a steady flow of nitrogen gas (99.99% pure) at a rate of 100 mL/min was maintained during the heating process.

Post-activation Treatment

After activation, the carbon samples were allowed to cool to room temperature inside the furnace while nitrogen flowed through them. The resulting activated carbons, known as BSAC600 (micro-sized, without ball milling) and N-BSAC600 (nano ball milled), were repeatedly washed with hot distilled water (60–70 °C) to remove any remaining acid and soluble contaminants, until the wash water reached neutral pH (~7.0).

In order to conduct additional characterisation and adsorption studies, the cleaned samples were finally placed in airtight containers after being oven dried for 12 hours at 110 °C.

2.3 Characterization

Scanning Electron Microscopy (SEM)

The produced adsorbents (BSAC600 and N-BSAC600) were subjected to surface morphology analysis using scanning electron microscopy (SEM, Model/Make if available).To study particle size, surface texture, and pore distribution, micrographs were obtained at various magnifications.

Fourier Transform Infrared Spectroscopy (FTIR)

Fourier transform infrared spectroscopy (FTIR) was used to identify functional groups on the adsorbents' surface. The presence of oxygenated, aromatic, and other surface functionalities important to dye adsorption was ascertained by analysing the distinctive absorption bands.

X-ray Photoelectron Spectroscopy (XPS)

X-ray photoelectron spectroscopy (XPS, Model/Make if available) was used to evaluate the elemental composition and chemical states of the surface. High-resolution spectra were deconvoluted for C 1s, O 1s, and other pertinent elements. Potential adsorption pathways were revealed by evaluating the O/C atomic ratio and surface oxygen functionality using the data.

2.4 Batch Adsorption Studies

The dye solution was prepared using Remazol Brilliant Orange 3R (C20H17N3Na2O11S3) dye, which has a maximum wavelength of 490 nm. To create a stock solution, a known quantity of Remazol Brilliant Orange 3R dye was dissolved in distilled water. By dilution, working solutions with the required concentrations were produced. 25–100 mL of dye solution at known initial concentrations were added to 250 mL Erlenmeyer flasks for batch adsorption experiments. The following parameters were systematically changed: initial dye concentration (100-200 mg/L), contact period (10–90 min), pH (1–10), adsorbent dosages (0.1–2.0 g), and temperature (30 °C, 40 °C, and 50 °C).

Procedure: 0.1 N HCl or 0.1 N NaOH were used to adjust the dye solution's pH. Using an orbital shaker, the mixtures were shaken for the designated contact time at 150–200 rpm. The solutions were filtered after adsorption, and a UV-Vis spectrophotometer set to λ_{max} = 490 nm was used to measure the amount of dye that remained. The dye removal percentage (%R) was calculated using the following formula

$$\% \text{ removal} = \frac{(C_0 - C_e)}{C_o o} \times 100 \qquad (2.4.1)$$

Where Co = initial dye concentration (mg/L), Ce = equilibrium dye concentration (mg/L) at time t. The adsorption capacity, q_e (mg/g), was computed using the following equation:

$$q_e = \left(\frac{C_0 - C_e}{M}\right) \times V \qquad (2..4.2)$$

Where C_o is the initial concentration of pollutants, C_e is the equilibrium concentration after adsorption (mg/L), V is the volume of solution (mL), and M is the mass of adsorbent (g).

Batch adsorption studies were carried out to evaluate the performance of BSAC600 and N-BSAC600 for the removal of Remazol Brilliant Orange 3R (RBO-3R) dye. All experiments were performed in 100 mL Erlenmeyer flasks containing 25-50 mL of dye solution at predetermined concentrations. A known dose of adsorbent was added to each flask, and the mixtures were agitated at a constant speed of 200rpm using an orbital shaker to ensure uniform suspension. At the end of the specified contact time, the suspensions were centrifuged, and the supernatant was analysed for residual dye concentration using a UV–Vis spectrophotometer at λmax = 494 nm.

The following para were systematically changed:

Effect of pH: The initial solution pH was adjusted from 1 to 10 using 0.1 M HCl or NaOH.

Effect of Initial Dye Concentration: Experiments were conducted with RBO-3R concentrations ranging from 100 to 200 mg/L.

Effect of Adsorbent Dose: Adsorbent dosages were varied between 0.1 to 2.0 g.
Effect of Contact Time: Samples were withdrawn at intervals between 10 to 90 minutes until equilibrium was attained.
Effect of Temperature: Adsorption experiments were performed at 30, 40, and 50 °C to evaluate the thermodynamic behaviors

2.5 Adsorption Isotherm, Kinetics, and Thermodynamics

Adsorption isotherms, kinetic models, and thermodynamic parameters were analysed.

To describe the adsorption behaviour of Remazol Brilliant Orange 3R (RBO-3R) onto BSAC600 and N-BSAC600.

Langmuir model

$$q_e = \left(\frac{q_{max} b C_e}{1+bC_e}\right) \quad (2.4.3)$$

where qe is the equilibrium adsorption capacity (mg/g), qmax is the maximum monolayer adsorption capacity (mg/g), b is the Langmuir constant (L/mg), and Ce is the equilibrium dye concentration (mg/L).

Freundlich model

$$q_e = K_F C_e^{1/n} \quad (2.4.4)$$

Where K_F ((mg/g)(L/mg)^(1/n)) is the Freundlich constant and 1/n is the heterogeneity factor [10].

KineticModels

The adsorption kinetics were analysed using pseudo-first-order, pseudo-second-order kinetic models [11].

Pseudo-first-order model (Lagergren)

$$\ln q_e - q_t = \ln q_e - k_1 t \quad (2.4.5)$$

where q_t is the adsorption capacity at time t (mg/g), and k_1 is the pseudo-first-order rate constant (min^{-1}).

Pseudo-second-order model

$$\frac{t}{q_t} = \frac{1}{k_2 q_e^2} + \frac{t}{q_e} \quad (2.4.6)$$

where k_2 is the pseudo-second-order rate constant (g/mg·min).[8]

Thermodynamic Studies

The effect of temperature on adsorption was studied to determine spontaneity and feasibility.

The enthalpy (ΔH°) and entropy (ΔS°) changes were estimated from the van't Hoff equation:

$$\ln K_c = \frac{\Delta H^o}{RT} + \frac{\Delta S^o}{R} \quad (2.4.7)$$

where R is the universal gas constant (8.314 J/mol·K) and T is the absolute temperature (K)[11]

III.RESULTS AND DISCUSSION

3.1 Fourier Transform Infrared Spectroscopy (FTIR) Analysis

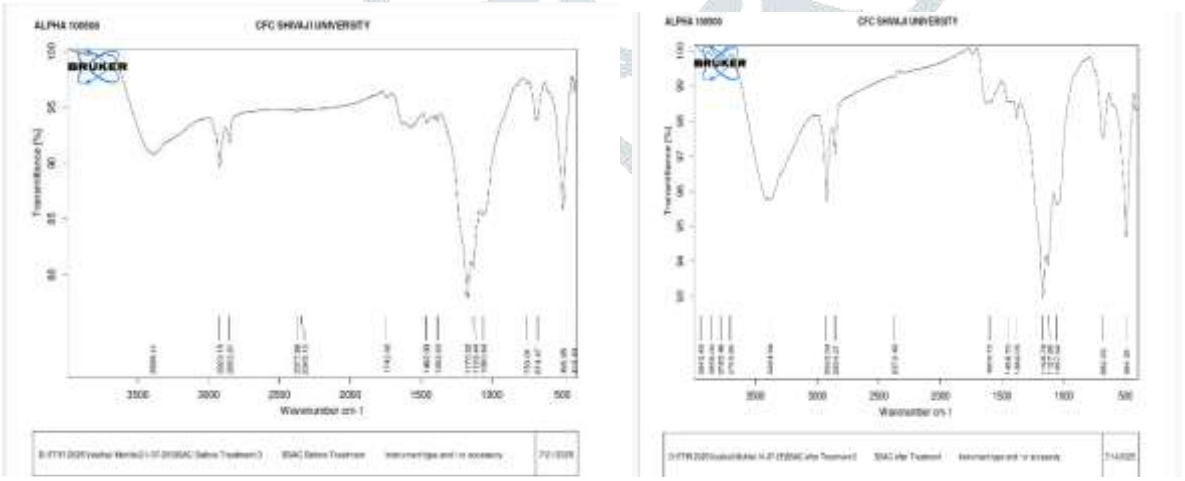

(a) **(b)**

Fig.1 FTIR spectra of BSAC600 (with nano ball milling) (a) before and (b) after adsorption

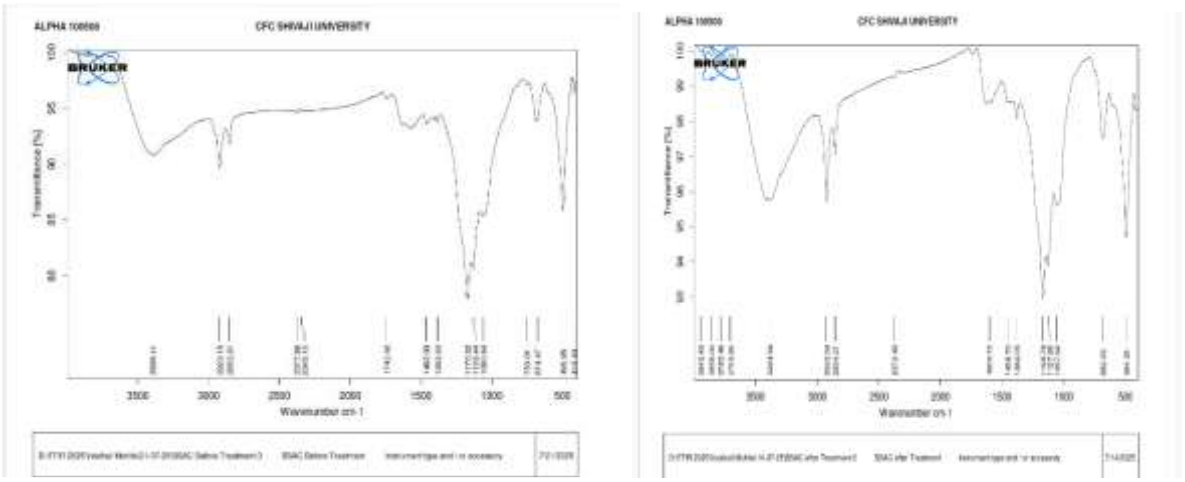

(a) (b)

(Fig.2 FTIR spectra of BSAC600 (micro, without nano ball milling) (a) before and (b) after adsorption

Table 1. Major FTIR peaks of BSAC600 and N-BSAC600 before and after RBO-3R adsorption

Adsorbent	Condition	Major Bands (cm^{-1})	Assignment	Observation after adsorption
BSAC600	Before adsorption	3398 (O–H), 2925–2852 (C–H), 1742–1657 (C=O), 1600 (C=C), 1227–1050 (C–O)	Hydroxyl, aliphatic, carbonyl, aromatic, ether	Decrease in O–H intensity, shift in C=O and C–O, new peaks in 900–700 cm^{-1}
BSAC600	After adsorption	Same bands, reduced intensities	Same	Functional group involvement in dye binding
N-BSAC600	Before adsorption	3726–3429 (O–H), 2924–2854 (C–H), 1742–1650 (C=O), 1580–1510 (C=C), 1227–1118 (C–O)	Hydroxyl, aliphatic, carbonyl, aromatic, ether	Stronger initial bands due to nanosizing
N-BSAC600	After adsorption	Same bands with major intensity reduction	Same	Stronger interactions with dye; new aromatic signals

3.2 Scanning Electron Microscopy (SEM) Analysis

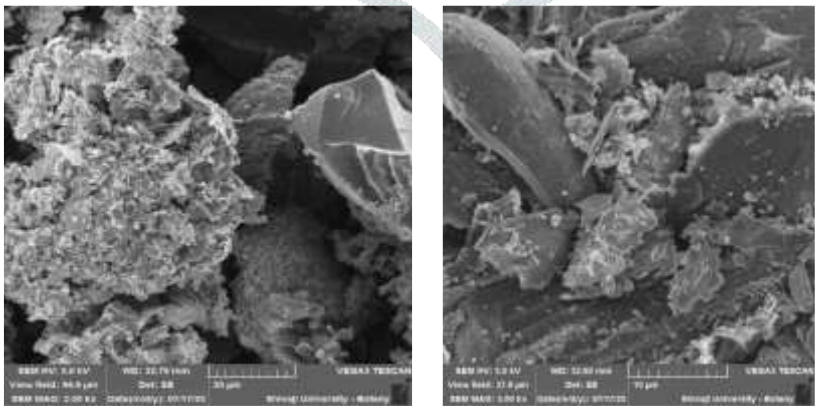

Fig.3 SEM (a) before and (b) after adsorption of BSAC at 600°C (without nano-milling)

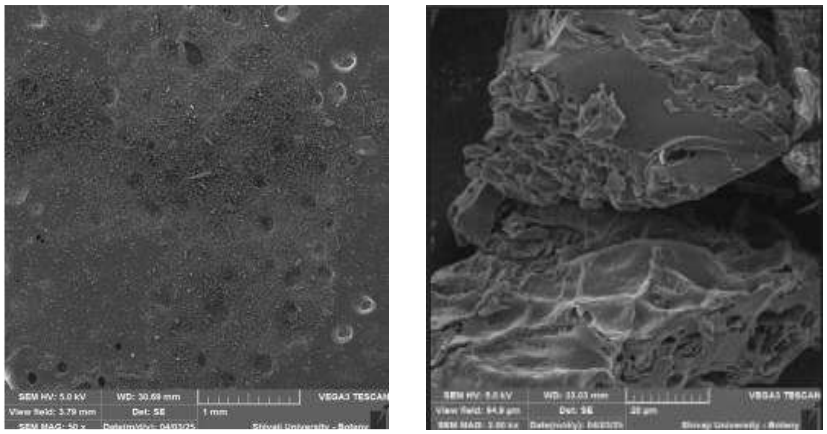

Fig. 4 SEM (a) before and (b) after adsorption of BSAC at 600 °C (nano-milling)

Fig. 3(a–b) represents SEM micrographs of BSAC600 (micro) and Fig. 4(a–b) N-BSAC600 (nano) before and after adsorption of Remazol Brilliant Orange 3R (RBO-3R).

Before adsorption, the surface of BSAC600 showed comparatively bigger and irregular particles with a compact structure and fewer exposed pores [Fig. 3a]. The porosity seemed limited, despite the presence of some apparent gaps and voids, which would limit the adsorption capacity. Deposition of RBO-3R onto the adsorbent surface was confirmed by the smoother surface shape and the appearance of many holes and cavities blocked by dye molecules upon adsorption [Fig. 3b].

In contrast, the N-BSAC600 micrographs [Fig. 4a] showed that nano ball milling produced a highly fragmented morphology with smaller particle sizes and coarser texture. There were numerous visible pores and channels, suggesting a higher exterior surface area and easier access to adsorption sites. Significant dye molecule surface coverage was seen upon adsorption [Figure Z4], with pore structures either partially filled or hidden.

In contrast, the N-BSAC600 micrographs [Fig. 4a] showed that nano ball milling produced a highly fragmented morphology with smaller particle sizes and coarser texture. There were numerous visible pores and channels, suggesting a higher exterior surface area and easier access to adsorption sites. Significant dye molecule surface coverage was seen upon adsorption [Fig. 4b], with pore structures either partially filled or covered [9].

3.3 X-ray Photoelectron Spectroscopy (XPS) Analysis

The surface elemental composition and chemical states of BSAC600 were determined by XPS analysis both prior to and following Remazol Brilliant Orange 3R (RBO-3R) adsorption. Fig. 5 a-d display the survey and high-resolution spectra for C 1s, O 1s, N 1s, S 2p, and P 2p, while Table 2 provides a summary of the corresponding atomic percentages [9].

```
Title              : 150535479 SpectrumScan Quantitative_MgKa.ssf
Date               : Thursday, June 19, 2025
Operator           : XPS User
Technique          : XPS
Source             : X-ray (MgKa) [1253.6eV]
Aperture Diameter  : 6 mm
Experiment         : Spectrum Scan : Quantitative
```

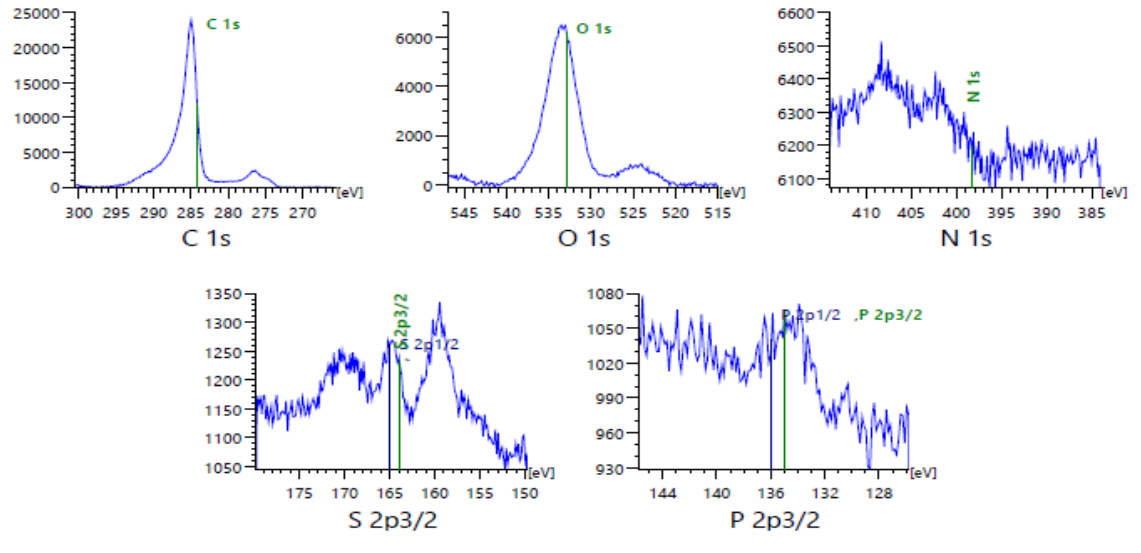

Element	Region	Start [eV]	Finish [eV]	Step [eV]	Dwell [ms]	Ep[eV]/IRR	Scans
C	1s	300.600	265.600	0.150	100	30	1
O	1s	547.000	515.000	0.150	100	30	2
N	1s	414.100	384.100	0.150	100	30	5
S	2p3/2	179.800	149.800	0.150	100	30	5
P	2p3/2	145.800	125.800	0.150	100	30	5

Element	State	Label	Sensitivity	Intensity (cps)	Atomic %
C	1s	C 1s	4.0789	812254.90	38.71
O	1s	O 1s	10.9556	337391.31	5.99
N	1s	N 1s	7.0410	1499877.00	41.41
S	2p3/2	S 2p3/2	7.1800	285195.00	7.72
P	2p3/2	P 2p3/2	5.1813	164257.50	6.16

Fig. 5 (a) XPS of BSAC600 before adsorption.

```
Title              : 104555069_SpectrumScan_Quantitative_MgKa.ssf
Date               : Friday, June 20, 2025
Operator           : XPS User
Technique          : XPS
Source             : X-ray (MgKa) [1253.6eV]
Aperture Diameter  : 6 mm
Experiment         : Spectrum Scan : Quantitative
```

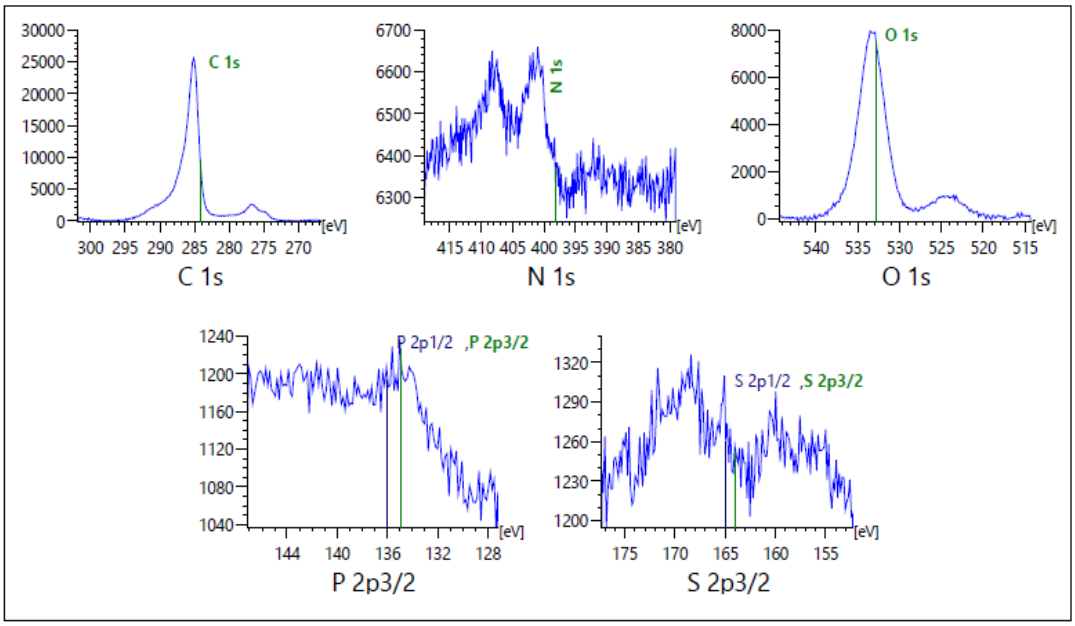

Element	Region	Start [eV]	Finish [eV]	Step [eV]	Dwell [ms]	Ep[eV]/IRR	Scans
C	1s	301.800	266.800	0.150	100	30	1
N	1s	419.100	379.100	0.150	100	30	5
O	1s	544.400	514.400	0.150	100	30	2
P	2p3/2	147.200	127.200	0.150	100	30	5
S	2p3/2	177.300	152.300	0.150	100	30	5

Element	State	Label	Sensitivity	Intensity (cps)	Atomic %
C	1s	C 1s	4.0789	854299.15	34.35
N	1s	N 1s	7.0410	2072532.00	48.27
O	1s	O 1s	10.9556	371426.76	5.56
P	2p3/2	P 2p3/2	5.1813	188947.50	5.98
S	2p3/2	S 2p3/2	7.1800	255850.50	5.84

Fig. 5(b) XPS of BSAC600 after adsorption

```
Title              : 150535479_SpectrumScan_Quantitative_MgKa.ssf
Date               : Thursday, June 19, 2025
Operator           : XPS User
Technique          : XPS
Source             : X-ray (MgKa) [1253.6eV]
Aperture Diameter  : 6 mm
Experiment         : Spectrum Scan : Quantitative
```

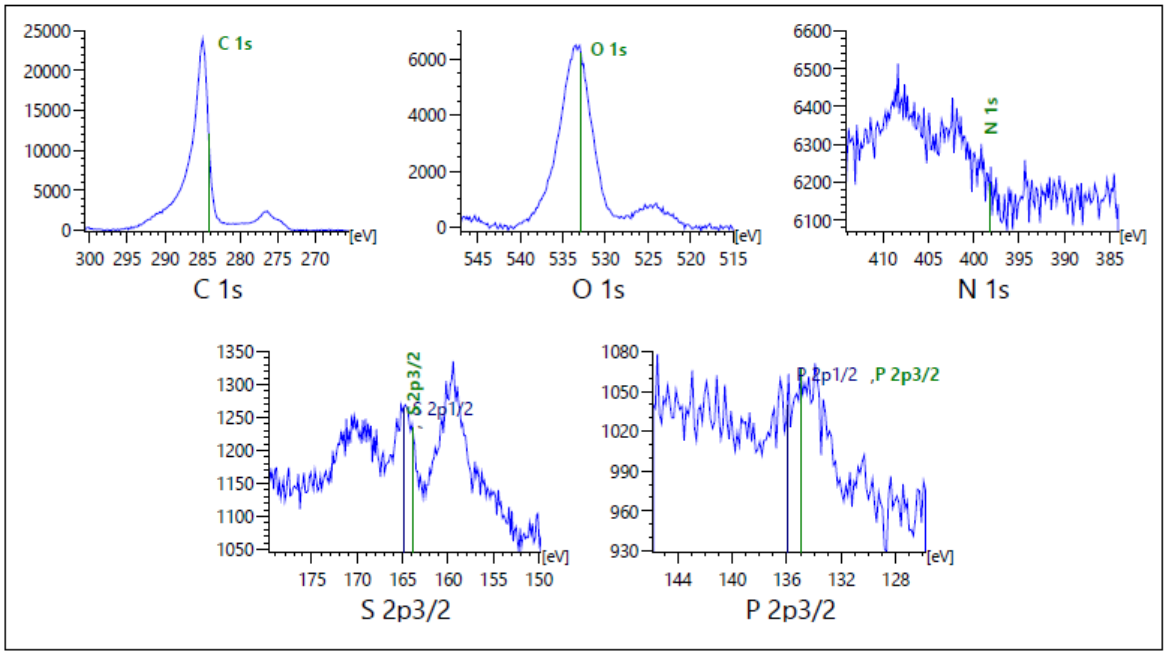

Element	Region	Start [eV]	Finish [eV]	Step [eV]	Dwell [ms]	Ep[eV]/IRR	Scans
C	1s	300.600	265.600	0.150	100	30	1
O	1s	547.000	515.000	0.150	100	30	2
N	1s	414.100	384.100	0.150	100	30	5
S	2p3/2	179.800	149.800	0.150	100	30	5
P	2p3/2	145.800	125.800	0.150	100	30	5

Element	State	Label	Sensitivity	Intensity (cps)	Atomic %
C	1s	C 1s	4.0789	812254.90	38.71
O	1s	O 1s	10.9556	337391.31	5.99
N	1s	N 1s	7.0410	1499877.00	41.41
S	2p3/2	S 2p3/2	7.1800	285195.00	7.72
P	2p3/2	P 2p3/2	5.1813	164257.50	6.16

Fig. 6(a) XPS for BSAC600 before adsorption (without nanoball milled)

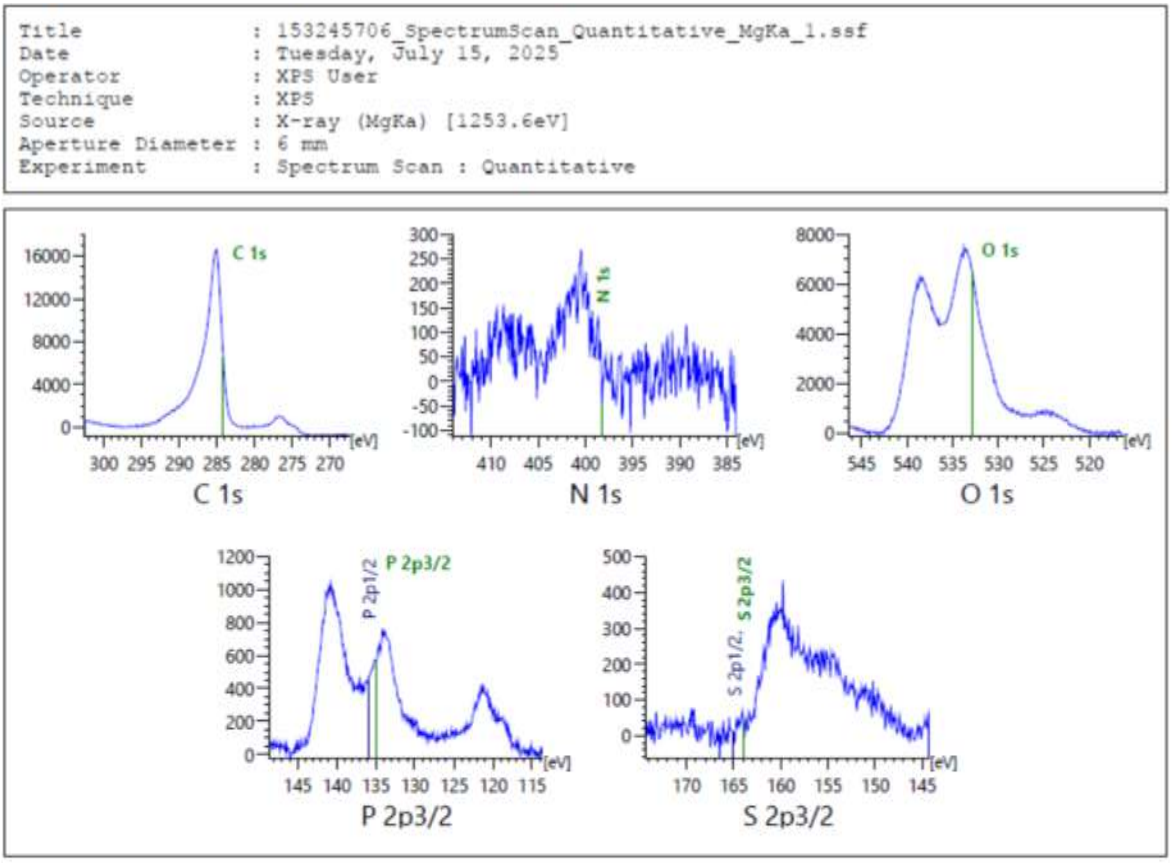

Element	Region	Start [eV]	Finish [eV]	Step [eV]	Dwell [ms]	Ep[eV]/IRR	Scans
C	1s	302.500	267.500	0.100	100	30	3
N	1s	414.100	384.100	0.100	100	30	3
O	1s	546.400	516.400	0.100	100	30	3
P	2p3/2	148.700	113.700	0.100	100	30	3
S	2p3/2	174.300	144.300	0.100	100	30	3

Element	State	Label	Sensitivity	Intensity (cps)	Atomic %
C	1s	C 1s	4.0789	506774.91	60.98
N	1s	N 1s	7.0410	14274.20	1.00
O	1s	O 1s	10.9556	600455.80	26.90
P	2p3/2	P 2p3/2	5.1813	96019.55	9.10
S	2p3/2	S 2p3/2	7.1800	29583.63	2.02

Fig. 6 (b) XPS for BSAC600 after adsorption (without nanoball milled)

Table 2. XPS atomic composition of BSAC600 before and after RBO-3R adsorption

Element	**Binding Region**	**Before adsorption (%)**	**After adsorption (%)**	**Observation**
C 1s	284.6 eV	38.71	60.98	Significant increase, confirming dye carbon deposition
O 1s	~532 eV	11.40	26.90	Increase due to oxygen-rich sulfonic groups of RBO-3R
N 1s	~400 eV	41.41	1.00	Decrease, dye adsorption alters the nitrogen environment
S 2p	165–170 eV	7.72	2.02	Adsorbed dye introduces sulfonic groups.
P 2p	~133 eV	6.16	9.10	Stable phosphorus peak from H_3PO_4 activation

3.4. Effect of Process Parameters on Dye Removal

3.4.1 Effect of pH

For both adsorbents, the pH of the solution has a significant impact on the percentage of the adsorbate that is removed. The acidic range (probably between pH 2-4) seems to be the ideal pH for adsorption, with removal efficacy declining as the pH gets more basic or neutral. Importantly, the removal effectiveness of the nanoform (At600CNB) is substantially better than that of the microform (At600CnonNB) over the whole pH range.

This pH dependence is typical of surface charge-influenced adsorption processes. Activated carbon made from bamboo usually has an acidic surface with functional groups that include oxygen (such as phenolic and carboxyl). The carbon's surface becomes protonated and gains a positive charge in acidic environments (low pH). This promotes anionic dye molecules' electrostatic attraction, which is typical of textile dyes like RBO 3R.

The nanostructure of At600C-NB is responsible for its outstanding performance. Compared to microparticles, nanoparticles have a significantly higher specific surface area (SSA) and more active sites per unit mass. The enormous surface area of the nano-carbon enables better interaction with and adsorption of dye molecules, even at less ideal pH conditions. Changes in electrostatic driving forces have a more significant impact on the micro-carbon because of its smaller SSA.

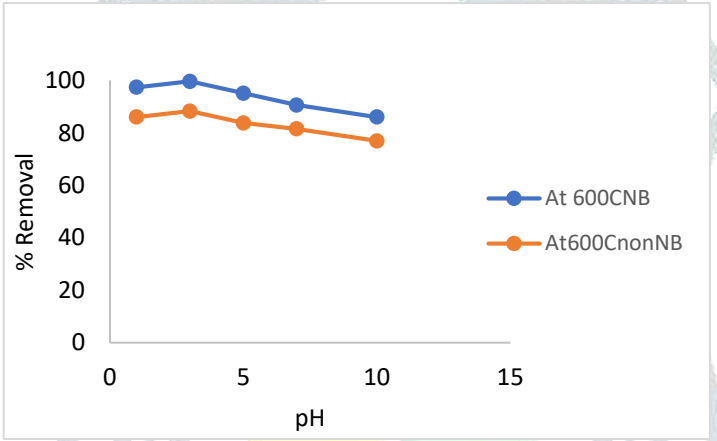

Fig.7 Effect of pH

3.4.2 Effect of adsorbent dose

With increasing doses of both adsorbents, the % removal of the adsorbate rises quickly before slowing down at higher doses(. Similar to the pH research, the nano-carbon (At600CNB) outperforms the micro-carbon in terms of removal percentage at all doses and reaches its maximum removal at a lower dose.

As additional adsorbent is introduced, more adsorption sites become available, which causes the initial sharp increase in removal. When all available sites are occupied and the dye concentration reaches equilibrium, it slows down at higher doses. Similar to the pH research, the nano-carbon (At600CNB) outperforms the micro-carbon in terms of removal percentage at all doses.

Surface area directly leads to this outcome. Compared to a greater mass of At600CnonNB, a smaller mass of At600CNB offers an equal or higher number of active sites.

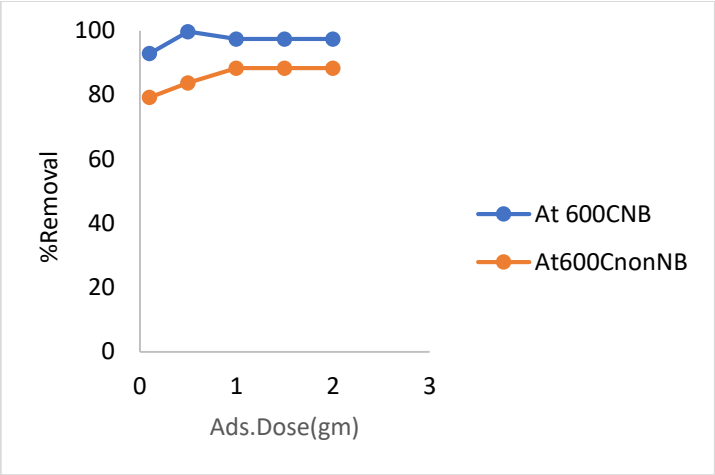

Fig.8 Effect of Ads. Dose.

3.4.3 Effect of contact time

For both materials, the adsorption occurs quickly in the first 20 to 40 minutes before progressively getting closer to equilibrium (Fig. 9). In addition to achieving a greater ultimate removal %, the nano-carbon (At600CNB) reaches equilibrium considerably more quickly than the micro-carbon. The large number of unoccupied surface places is what caused the quick initial uptake. Because of slower pore diffusion and repulsive forces between molecules in the solution and those already adsorbed, the rate decreases as these sites fill. One significant benefit of At600CNB is its quicker kinetics. This can be clarified by:

Reduced Intraparticle Diffusion Path Length: Compared to bigger microparticles, a dye molecule must diffuse into a pore over a much shorter distance in nanoparticles. Internal mass transfer resistance is lowered as a result. Greater Surface Area: Rapid initial adsorption is made possible by the greater exterior surface area, which offers instant access to a large number of sites. When building continuous flow systems where efficiency demands a short residence time, this property is essential.

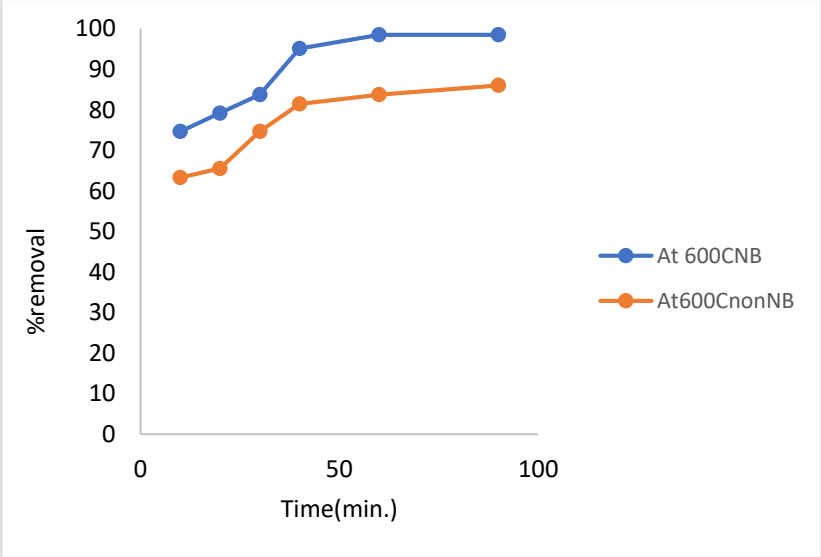

Fig.9. Effect of Time

Fig. 11 illustrates how the initial concentration of RBO-3R dye affects The % removal falls as the dye's initial concentration rises, but the actual adsorption capacity (q, mg dye adsorbed per gram of adsorbent) rises. With a sharper increase in capacity and a higher removal percentage at all concentrations, the nano-carbon (At600CNB) continuously performs better than the micro-carbon. High percentage removal results from a high ratio of accessible adsorption sites to dye molecules at lower concentrations. The sites become saturated, and the % removal decreases as the concentration rises. However, more dye molecules are forced onto the adsorbent by the stronger mass transfer driving force provided by the larger concentration gradient, increasing the capacity (q) until the absolute maximum capacity is attained.

3.4.4 Effect of temperature:

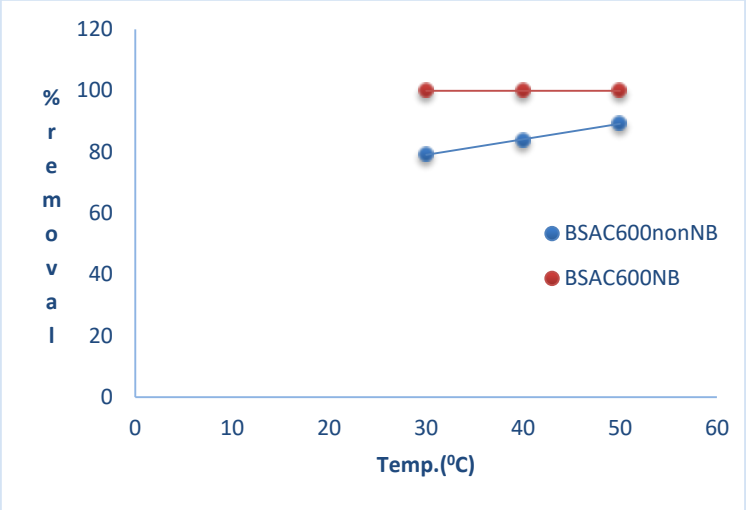

Fig.10. Effect of Temperature

The effect of temperature on Remazol Brilliant Orange-3R (RBO-3R) adsorption onto BSAC600 (micro, non-milled) and N-BSAC600 (nano ball-milled) was examined between 30 and 50 °C (Fig. 10). The percentage of dye removed for both adsorbents increased slightly with increase in temperature, suggesting that adsorption was endothermic. The dye removal efficiency of BSAC600 (micro) rose from about 78% at 30 °C to about 88% at 50 °C. Increased mobility of dye ions at higher temperatures and improved diffusion of dye molecules into the pores could be the cause of this improvement. However, the total removal was still less than that of the nano equivalent, indicating that the micro-structured adsorbent had fewer accessible adsorption sites. On the other hand, N-BSAC600 (nano) continuously produced almost total elimination (~99%) at all temperatures examined, with very little fluctuation. The observed pattern suggests that the adsorption process is less susceptible to temperature impacts since the nano ball-milled adsorbent has a large number of active sites and a significant affinity for RBO-3R. Overall, the results suggest that N-BSAC600 has already reached optimum performance regardless of temperature fluctuation, whereas BSAC600 (micro) demonstrated better removal efficiency with rising temperature.

3.4.5 Effect of Initial Concentration

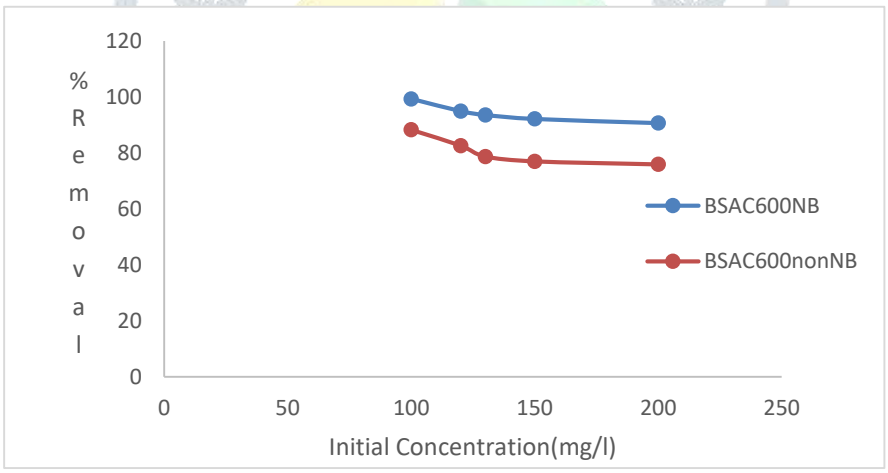

Fig. 11 Effect of Initial Concentration

Fig. 11 illustrates how the initial concentration of RBO-3R dye affects the adsorption by BSAC600 (micro, non-milled) and N-BSAC600 (nano ball-milled). Both adsorbents had a gradual decrease in percentage removal as the dye concentration increased from 100 to 200 mg/L whereas BSAC600 The dye removal efficiency of BSAC600 (micro) decreased from about 87% at 100 mg/L to about 77% at 200 mg/L. At greater concentrations, when there are more dye molecules in solution than there are active sites on the adsorbent surface, the available adsorption sites become saturated, which is the cause of this pattern. (micro) saw a more noticeable decline

The removal effectiveness of N-BSAC600 (nano), on the other hand, was continuously higher, sustaining ~98–92% over the same concentration range. The FTIR and XPS investigations verified that N-BSAC600's superior performance can be attributed to its increased exposure of oxygen functional groups, improved surface roughness, and reduced particle size. These characteristics allowed for improved active site usage and stronger dye–adsorbent interactions, even at high concentrations.

Overall, the findings show that N-BSAC600 had a greater resistance to concentration effects and a stronger capacity for dye uptake, even if site saturation caused adsorption efficiency to decline for both adsorbents as concentration increased. This conclusion is corroborated by isotherm analysis, which showed that the nano ball-milled adsorbent had a significantly larger maximum adsorption capacity (qmax) than its micro-sized counterpart according to the Langmuir model [13,14,15,16].

3.5 Adsorption Isotherm Studies

The equilibrium interaction between the RBO-3R dye molecules and the adsorbents was assessed using adsorption isotherm models. For BSAC600 (micro) and N-BSAC600 (nano), both Langmuir and Freundlich models were investigated; the findings are displayed in Figures A–D, and Table 3 provides a summary of the relevant parameters.

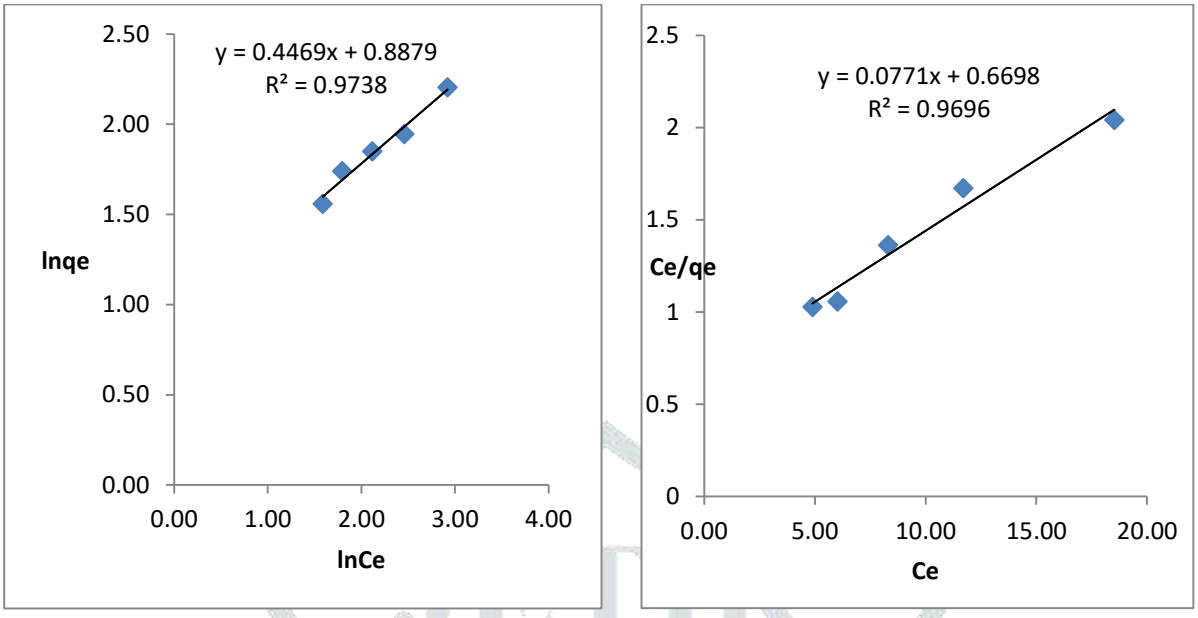

(a) (b)

Fig.12 Adsorption isotherm models for N-BSAC600 (nano),(a) Freundlich (b) Langmuir

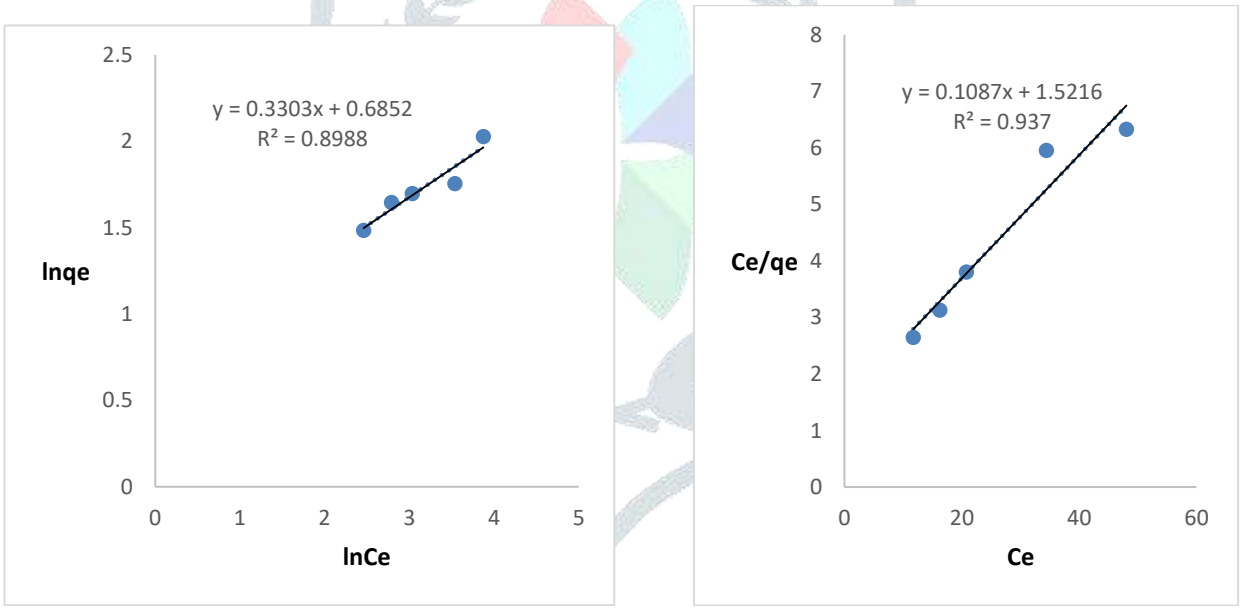

(c) (d)

Fig.12 Adsorption isotherm models for N-BSAC600 (micro),(c) Freundlich (d) Langmuir

Langmuir Isotherm

Monolayer adsorption on a uniform surface with finite binding sites is assumed by the Langmuir model. The plots of Ce/qe vs produced strong correlation coefficient linear connections for both adsorbents (R^2 = 0.937 for BSAC600 and 0.9696 for N-BSAC600). The highest adsorption capacity (qmax) was noticeably greater for N-BSAC600, indicating that nano ball milling increased the availability of adsorption sites and raised the effectiveness of dye uptake. Stronger binding affinity of RBO-3R to N-BSAC600 was also shown by the greater Langmuir constant (b) [17,17,19,20].

Freundlich Isotherm

Multilayer adsorption on heterogeneous surfaces is described by the Freundlich model. The lnqe vs lnCe also provided a decent fit to the data (R^2 = 0.8988 for BSAC600 and 0.9738 for N-BSAC600). Favourable adsorption was indicated by the Freundlich constant (n > 1) for both adsorbents; N-BSAC600 displayed a greater slope value, indicating improved surface heterogeneity and improved interaction with dye molecules.

The Langmuir model showed a marginally superior correlation for both adsorbents, indicating that monolayer adsorption was the predominant process, even though both models offered respectable fits. Significantly, N-BSAC600's better performance in the Freundlich and Langmuir models suggests that surface heterogeneity and extra adsorption sites were revealed by nano ball milling, which enhanced the dye's ability to absorb dye and its adsorption strength [8,9,14,21,22].

Table 3. Langmuir and the Freundlich isotherm parameters for RBO-3R adsorption onto BSAC600 and N-BSAC600

Adsorbent	Langmuir R^2	qmax (mg/g)	KL (L/mg)	Freundlich R^2	n	Kf (mg/g)
BSAC600 (micro)	0.937	9.20	0.071	0.8988	3.03	1.98
N-BSAC600 (nano)	0.9696	12.97	0.115	0.9738	2.24	2.43

3.6 Thermodynamic analysis

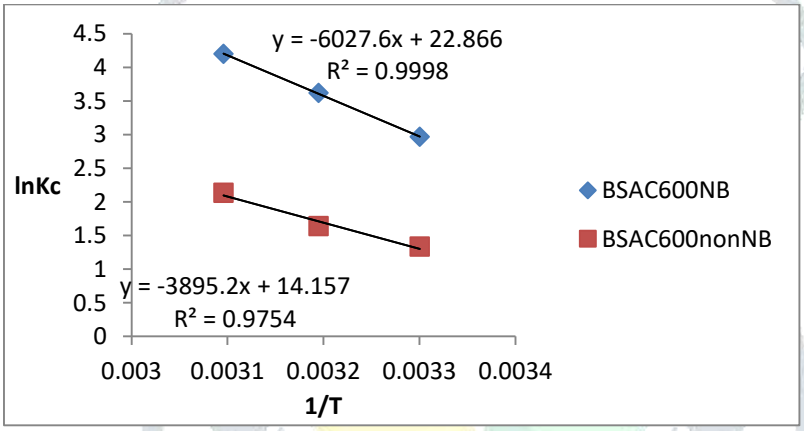

Fig.13 Thermodynamic analysis

Table 4. Thermodynamic parameters for RBO-3R adsorption onto BSAC600 micro and nano adsorbents

Adsorbent	ΔH° (kJ/mol)	ΔS° (J/mol·K)	ΔG° at 303 K (kJ/mol)	Nature
BSAC600 non-NB (micro)	+32.4	+117.7	–3.3	Spontaneous, Endothermic
BSAC600 NB (nano)	+50.1	+190.2	–7.6	Spontaneous, Endothermic

Table 4 provides a summary of the thermodynamic characteristics for RBO-3R adsorption onto BSAC600 (micro) and N-BSAC600 (nano). The endothermic character of the adsorption process was confirmed by the positive ΔH° values (32.4–50.1 kJ/mol) displayed by both adsorbents. Increased randomness at the solid-liquid interface is suggested by positive ΔS° values (117.7–190.2 J/mol·K), which are probably caused by dye molecule decomposition and strong adsorbent–adsorbate interactions.

At all assessed temperatures, negative ΔG° values verified that adsorption was both spontaneous and thermodynamically possible. Additionally, the higher spontaneity and better affinity of the nano ball-milled adsorbent toward RBO-3R are shown by the larger negative ΔG° values for N-BSAC600 (–7.6 kJ/mol at 303 K) in comparison to BSAC600 (–3.3 kJ/mol). The increased ΔH° and ΔS° values for N-BSAC600 further imply that nano ball milling improves structural heterogeneity and surface activity, leading to more robust adsorbent–dye interactions. These results are in line with kinetic and isotherm investigations, which demonstrated the nano adsorbent's faster kinetics and greater adsorption capacity [15,16,17,21,22].

3.7 Adsorption Kinetics

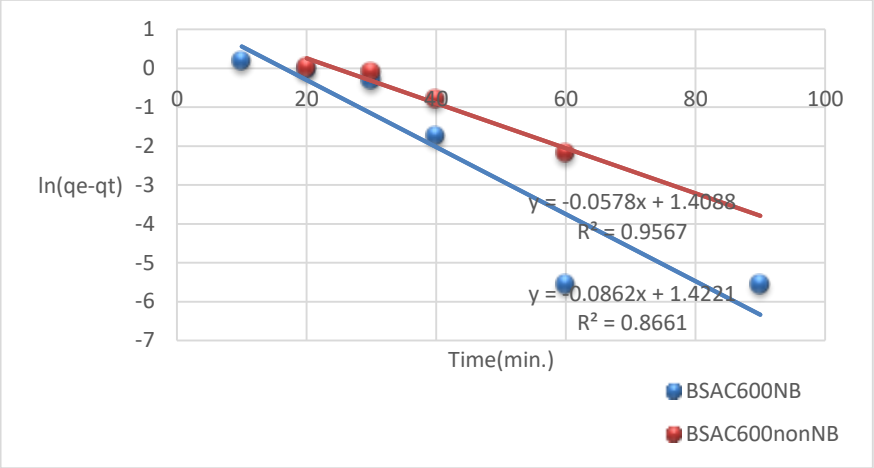

Fig.14(a) Kinetic data for pseudo 1st order BSAC 600 nano and micro.

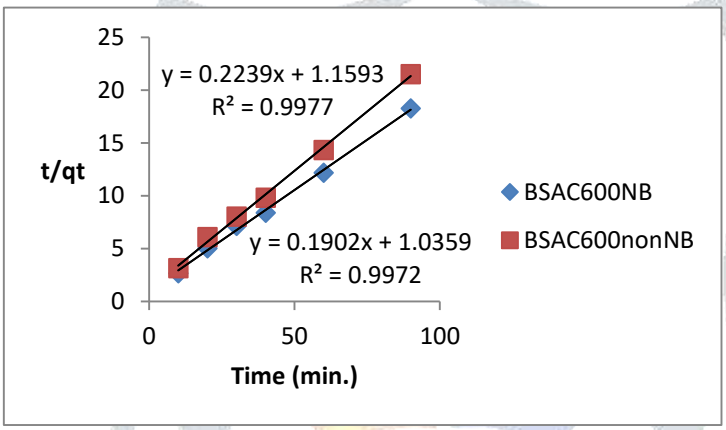

Fig.14(b) Kinetic data for Pseudo 2nd order BSAC 600 nano and micro.

To study the adsorption kinetics of RBO-3R onto BSAC600 (both non-milled and nano-ball milled), pseudo-first-order (PFO) and pseudo-second-order (PSO) models were used. With stronger correlation values (R2 = 0.9972 for BSAC600NB and 0.9977 for BSAC600nonNB) than the PFO model (0.8661 and 0.9567, respectively), the PSO model offered a better fit. The experimental q_e values (4.98 and 4.19 mg/g, respectively) and the PSO model's estimated equilibrium adsorption capacities ($q_e$calc) (5.26 mg/g for BSAC600NB and 4.47 mg/g for BSAC600nonNB) were nearly identical. In contrast, adsorption was understated by the PFO. model. These findings imply that chemisorption is the primary rate-controlling mechanism and validate that the adsorption process follows pseudo-second-order kinetics. Significantly, compared to its non-milled counterpart, the nano-ball-milled BSAC (BSAC600NB) demonstrated faster kinetics and a larger adsorption capacity, underscoring the advantageous impact of nano-milling in improving surface accessibility and active sites for dye removal[15,16,17,23,24,25].

Table 5. Kinetic Parameters

Sample	Model	q_e,exp (mg/g)	q_e,calc (mg/g)	k_1 or k_2	R^2
BSAC600NB (Nano)	PFO	4.98	4.15	k_1 = 0.0862 min^{-1}	0.8661
BSAC600NB (Nano)	PSO	4.98	5.26	k_2 = 0.0343 $g \cdot mg^{-1} \cdot min^{-1}$	0.9972
BSAC600nonNB (Micro)	PFO	4.19	4.09	k_1 = 0.0578 min^{-1}	0.9567
BSAC600nonNB (Micro)	PSO	4.19	4.47	k_2 = 0.0417 $g \cdot mg^{-1} \cdot min^{-1}$	0.9977

Overall, the comparative analysis shows that by improving the bamboo stick activated carbon's adsorption capacity (qmax), equilibrium uptake (q_e), and surface activity, nano-ball milling (BSAC600NB) enhances its adsorption performance. Thermodynamic data suggest that the nano-milled sample exhibits much greater adsorption efficiency, faster kinetics, and stronger dye–adsorbent interactions, even though both adsorbents exhibit pseudo-second-order kinetics and Langmuir isotherm behaviour. These enhancements confirm nano-milling as a viable modification method to maximise adsorbents made from biomass for wastewater treatment [26].

IV. CONCLUSION

This study compared the non-ball-milled (BSAC600nonNB) and nano-ball-milled (BSAC600NB) forms of bamboo stick activated carbon (BSAC), which was synthesised at 600 °C, for the adsorption of Remazol Brilliant Orange-3R (RBO-3R) dye in batch mode. SEM, FTIR, and XPS characterization data verified that nano ball milling enhanced dye–adsorbent interactions by reducing particle size, improving surface roughness, and adding more oxygen-containing functional groups. Important factors like pH, initial concentration, contact time, dosage, and temperature have a substantial impact on removal efficiency, according to batch adsorption trials. In comparison to the non-milled version, the nano-ball-milled adsorbent continuously showed better performance, attaining higher equilibrium capacity (q_e) and dye removal percentages

Adsorption was shown to follow the pseudo-second-order model by kinetic modelling, indicating chemisorption as the predominant process. The maximal monolayer capacity (qmax) for BSAC600NB was around 12.97 mg/g, while for BSAC600nonNB it was approximately 9.19 mg/g. Isotherm tests revealed that the Langmuir model offered the greatest fit. Stronger driving forces were seen for BSAC600NB, and thermodynamic analysis verified that the adsorption was endothermic ($\Delta H° > 0$), spontaneous ($\Delta G° < 0$), and accompanied by greater randomness at the solid–liquid interface ($\Delta S° > 0$).

Overall, it turned out that using nano ball milling to improve the adsorption effectiveness of activated carbon derived from bamboo was a successful modification technique. An environmentally benign, economical, and sustainable adsorbent for removing textile dyes is BSAC600NB. Regeneration performance, column studies, and testing with actual textile effluents should be the main areas of future research to evaluate broad applicability.

V. ACKNOWLEDGEMENT

We owe special thanks to the management and administration of Shivaji University, Kolhapur, Maharashtra, India for providing us with infrastructure for research work.

REFERENCES

[1] Brüschweiler, B. J., & Merlot, C. (2017). Azo dyes in clothing textiles can be cleaved into a series of mutagenic aromatic amines. Journal of Environmental Science and Health, Part C, 35(1), 1-30.
[2] Lellis B., et al. (2019). Effects of textile dyes on health and the environment. Biotechnology Research and Innovation, 3(2), 275-290.
[3] Holkar, C. R., et al. (2016). A critical review of textile wastewater treatments. Journal of Environmental Management, 182, 351-366.
[4] Teshale A, Amare T. A, Esayas A (2021) Textile Industry Effluent Treatment Techniques. Journal of Chemistry, Article ID 5314404,1-14, https://doi.org/10.1155/2021/531440
[5] Qanytah, K., Syamsu, K., Fahma, F., & Pari, G. (2020). "Characterization of ball-milled bamboo-based activated carbon treated with $KMnO_4$ and KOH as activating agents." BioResources, 15(4), 8303-8322
[6] .Foo K. Y., & Hameed, B. H. (2010). Insights into the modelling of adsorption isotherm systems. Chemical Engineering Journal, 156(1), 2–10. https://doi.org/10.1016/j.cej.2009.09.013.
[7] Hassan, S. S., Khong, H. Y., & Chang, Y. H. R. (2023). Facile preparation of scalable bamboo-derived activated carbon for efficient wastewater treatment. *BioResources*, 18(3), 5029–5045.
[8] Yao, Y., Zhou, X., Zhao, Y., & Liu, H. (2024). Efficient dye adsorption of mesoporous activated carbon from bamboo parenchyma cells by phosphoric acid activation. *RSC Advances*, 14(32), 18122–18132.
[9] Gao, P., Fan, X., Sun, D., Zeng, G., Wang, Q., & Wang, Q. (2024). Recent advances in ball-milled materials and their applications for the adsorptive removal of aqueous pollutants. *Water, 16*(12), 1639. https://doi.org/10.3390/w16121639
[10] Dutta, B.K. (2007), Principles of mass transfer and seperation processes, PHI Learning Pvt. Ltd.
[11] Ahmad, R. and Kumar, R. (2010) "Adsorptive removal of congo red dye from aqueous solution using bael shell carbon". Applied Surface Science 257(5), 1628-1633.
[12] Bagbi, Y., Khan, I., Soni, S., & Pandey, R. A. (2024). Waste bamboo-derived magnetically separable activated carbon for efficient dye adsorption: Characterization and mechanism insights. *Environmental Nanotechnology, Monitoring & Management*, 22, 100764.
[13] Nasrullah, A., et al. (2021). Effect of short time ball milling on physicochemical and adsorption performance of activated carbon prepared from mangosteen peel waste. *Renewable Energy, 173,* 417–428. https://doi.org/10.1016/j.renene.2021.03.056
[14] Saidi, M., Khelifa, A., & Benhabiles, O. (2025). Kinetics, thermodynamics and adsorption study of raw and treated diatomite as sustainable adsorbents for crystal violet dye. *Scientific Reports*, 15, 10545.
[15] Jie K., Haiting Z., Jiale Gao a, Yan Fang , Jiaqi Shi, Tao Geb, Ting Fanc, Yanhong Shi , Rong Zhang , Ningyuan Zhang , X inju Dong , Yunhua Zhanga, Hui Li. (2023). Mechanisms and adsorption capacities of ball-milled biomass fly ash/biochar composites for methylene blue adsorption. *Journal of Water Process Engineering, 55,* 104072. https://doi.org/10.1016/j.jwpe.2023.104072
[16] Wang, J., Yunfeng Tan, Hongjun Yang, Lingling Zhan, Guowen Sun, & Le Luo1 (2023). Adsorption characteristics and mechanism of ball-milled biochar for methylene blue removal. *Scientific Reports, 13,* 15231. https://doi.org/10.1038/s41598-023-42211-9
[17] Wang, B., et al. (2024). Ball milling and magnetic modification boosted methylene blue removal. *Nanomaterials, 14*(7), 1517. https://doi.org/10.3390/nano14071517

[18] Chen, C., Fengxia Y., Yongfei M., Lihong D., Zulin Z., Haixin G. and Yongzhen D. (2024). Ball milling boosted magnetic cotton husk-derived biochar for adsorption of oxytetracycline and ciprofloxacin from water, Carbon Research,63, https://doi.org/10.1007/s44246-024-00146-9

[19] LanqingLi, Yue X., Keyan C., Jun Z. MinW., WenqiangW., Zhifan Z., Fan Lu, Yadong D., and Yinghao F. (2024). Adsorption characteristics of ball milling-modified Chinese biochar residues. *ACS Omega*, *9*(4), 11658-11670. https://doi.org/10.1021/acsomega.3c09016

[20] Elena L., Gianluca V., Aida K., Yasser B., Maria A.,, Giuliana G. (2024). Efficiency of dye adsorption of modified biochar: Ball milling assisted activation, *Biomass and Bioenergy 185 (22),* 101151. https://doi.org/10.1016/j.biombioe.2024.107247

[21] Jingqi W., Tongshuai W., Shijia Li., Wei T., Shuhan Y., Zilong Z., Jiawei C. (2024). A green method to improve the adsorption capacity of hydrochar via ball milling. Carbon Research 3:60,1-16. https://doi.org/10.1007/s44246-024-00145-w

[22] Irene C., Riccardo G., Francesca M., Cristina M. (2025). Advances in biochar production and ball milling modification: A comprehensive review. Nano Trends 10 100117,1-16. https://doi.org/10.1016/j.nwnano.2025.100117

[23] Huang, R., Chaoting G., Qin G., Jin J. (2025). Ball-milling treated superfine powdered activated carbon triggers Mn(VII) activation for enhanced oxidation. *Water Research, 286,* 124255. https://doi.org/10.1016/j.watres.2025.124255

[24] Ptaszyńska, K., Anna M., Katarzyna M. E., José L. F.,Mieczysław K. (2024). Promoting effect of ball milling on functionalization of biochar and composite formation. *Molecules, 29*(3), 687. https://doi.org/10.3390/molecules29030687

[25] Yicheng Y., Yongshan W., Jianjun C., Hao C., Yuncong Li., Rafael M.C. , Yulin Z., Jinsheng H., Yue Z., Bin G. (2025). Ball-milled spent coffee ground biochar for effective adsorption of contaminants from water. *Water, 17,* 881.,1-16. https://doi.org/10.3390/w17060881

[26] Sanz-Santos, E., Ariadna Alvarez-Montero , Almudena G-A., Carolina B., Jorge B. (2025). Adsorption of modified polystyrene nanoplastics on biomass-derived activated carbons prepared by ball milling activation.Journal of Environmental Management, 391(1), 126654,1–11. https://doi.org/10.1016/j.jenvman.2025.126654